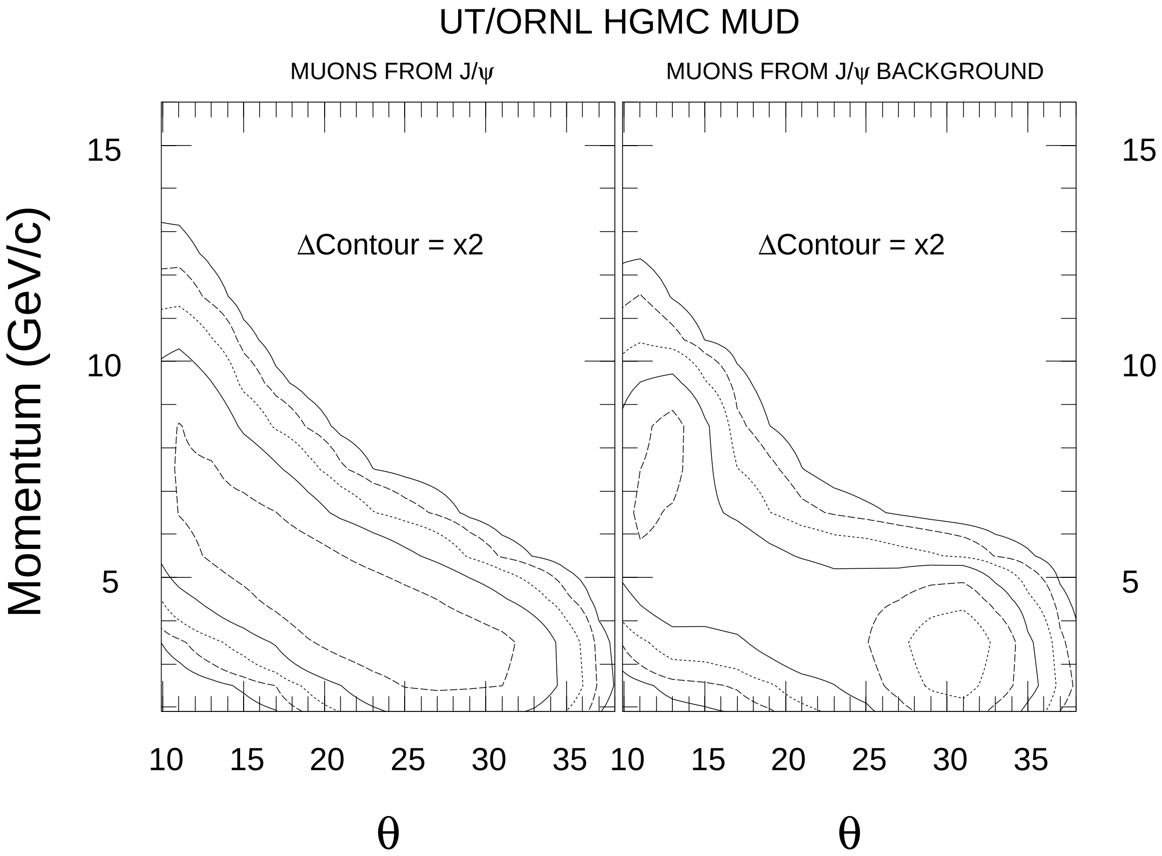

Figure 10.36: Contour plots of the $(P,\,\theta)$ distributions of accepted muons from J/ψ decay and the J/ψ background.

Trigger Implications

Elsewhere in this chapter the design of a muon trigger is described. Here the effectiveness of a simple LVL-1 muon pair trigger is demonstrated. Figure 10.40 shows the p_T distributions of pions and muons at various positions through the muon detector. These single particle yields form the basis for Fig. 10.7, which shows the fraction of central events with a) at least one accepted muon above a particular energy (upper figure) or b) at least one accepted muon pair above the invariant mass plotted. Note that even without any momentum measurement from the spectrometer, which would require a LVL-2 trigger, the pair trigger rate is less than 6% of all central events. Since we wish to record events with at least one accepted muon pair and the central event collision rate is around 1.5 kHz at nominal luminosity, we need only cope with a dimuon trigger rate of 100 Hz, which should pose no problem. For noncentral events the effectiveness of the simple dimuon trigger is even better as shown in Fig. 10.8.

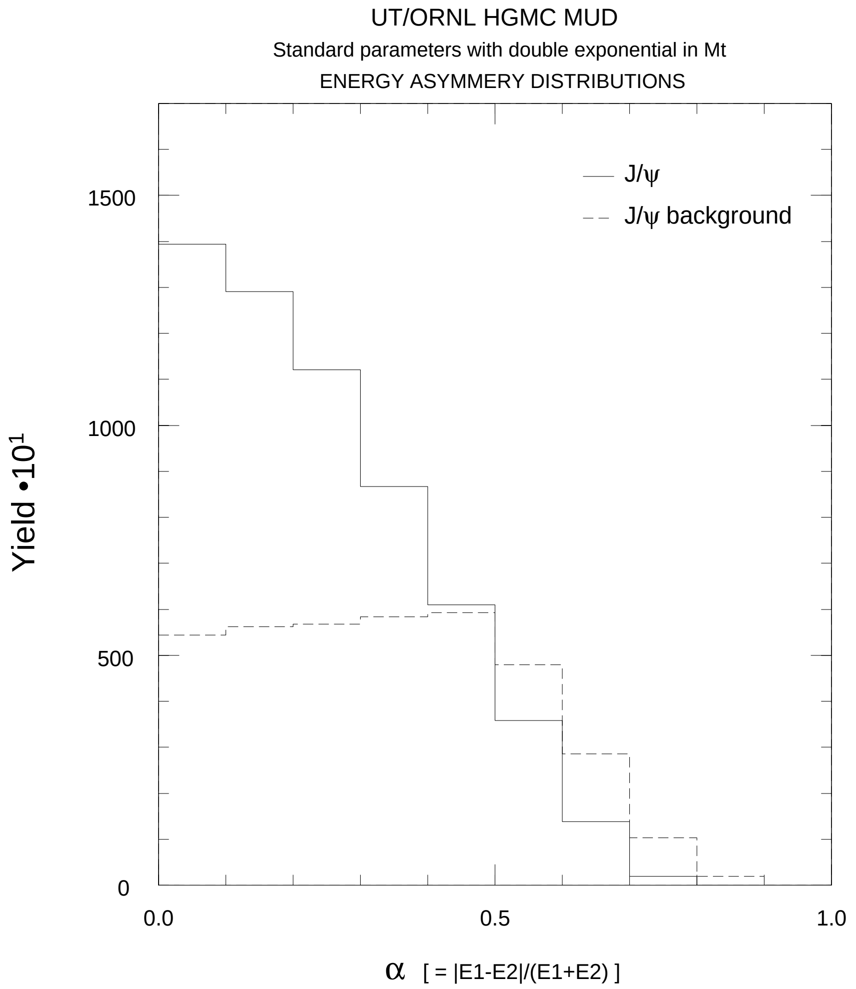

Figure 10.37: Yield distributions of the energy asymmetry parameter for dimuon origination from J/ψ-decay and from the resonance background, respectively.

This figure shows the fraction of events with a) one accepted muon, b) two accepted muons, c) two accepted unlike-sign muon and d) true pair muons as function of the neutral pion rapidity density.

10.4.5 Muon–Electron Coincidence Measurements

Charm production and decay is an important issue at RHIC, for at least two reasons: First, the measurement of "thermal" charm production has recently been suggested as a possible diagnostic of quark-gluon-plasma formation [8]. Also, copious semileptonic decays of charmed meson pairs produce a large opposite sign dilepton signal, which could obscure the

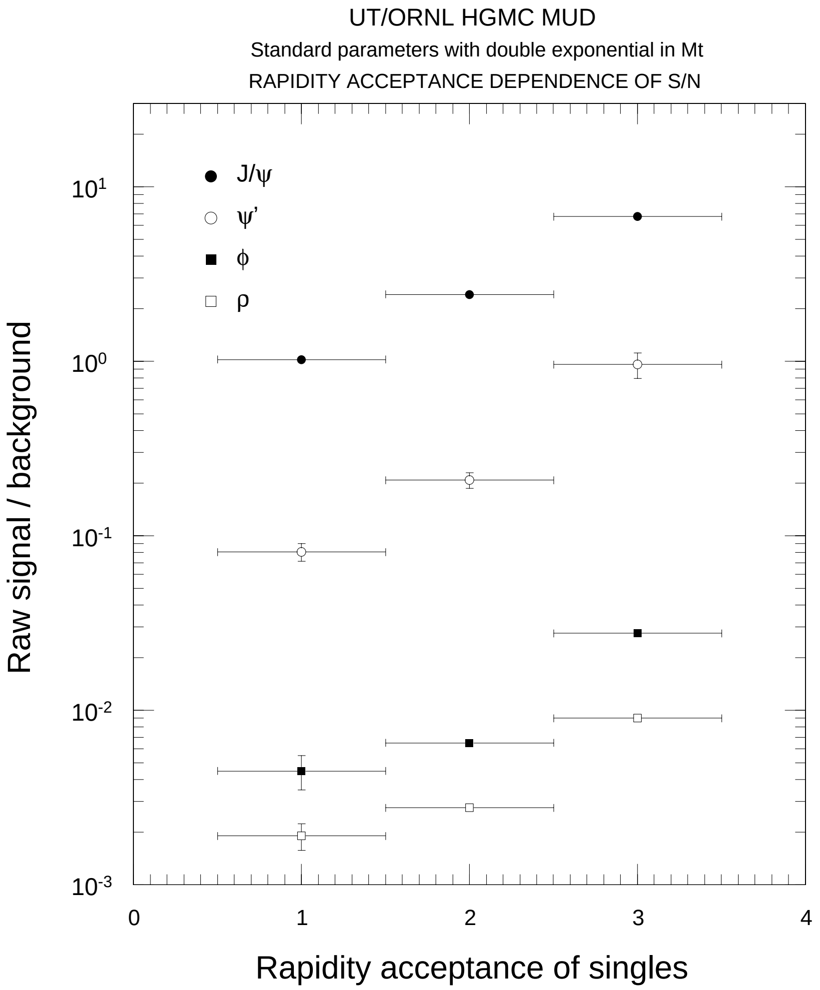

Figure 10.38: Variation of S/N for three muon detectors with rapidity acceptance 1 ± 0.5, 2 ± 0.5, and 3 ± 0.5, respectively. The S/N increases significantly for a more forward acceptance.

direct observation of "thermal" dilepton production in the plasma. $D\overline{D}$ production is highly correlated and semileptonic decays form opposite-sign lepton pairs with properties similar to those produced by the Drell–Yan mechanism.

Charm decays are predicted to dominate the e^+e^- and $\mu^+\mu^-$ mass spectra in the mass region below 4 GeV/c^2. Preliminary results from E789 [9] confirm this for the continuum below the J/ψ mass at $x_F \approx 0$. Consequently, charm production is an important component of the signal in the mass region where J/ψ suppression by color screening and thermal production of lepton pairs are expected. It is essential to understand the charm contribution quantitatively.

The major difference between the charm decay leptons and Drell–Yan pairs lies in the

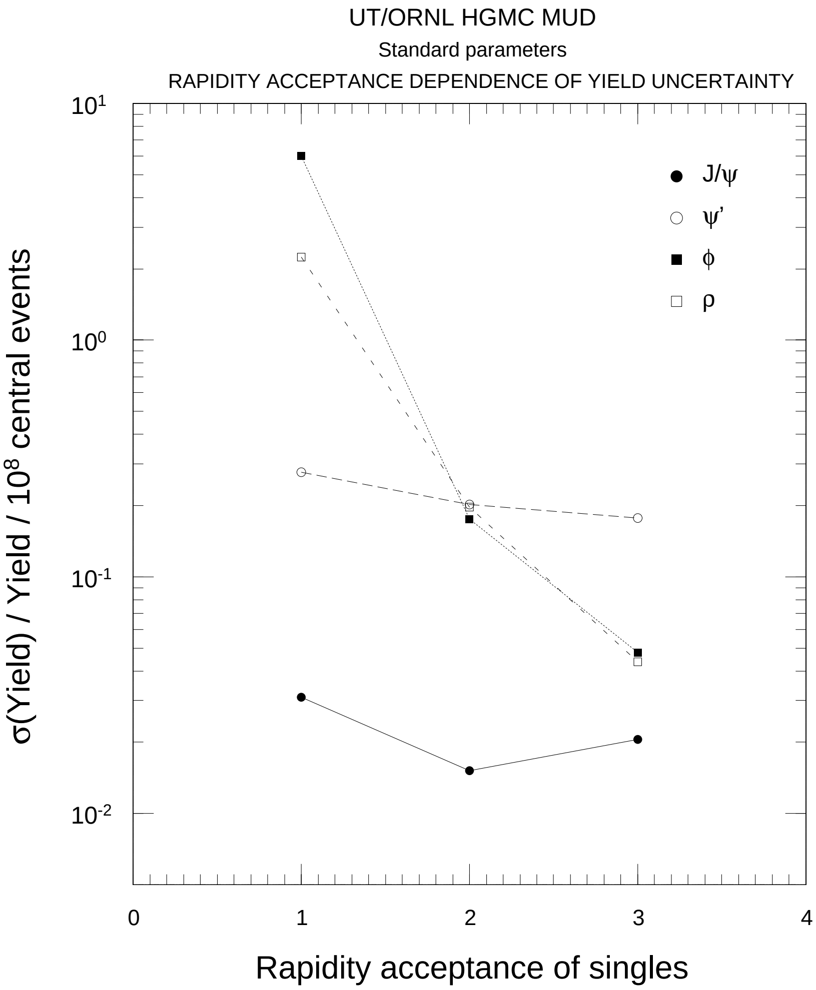

Figure 10.39: Variation of the relative yield uncertainty for the same three rapidity acceptances as in the previous figure.

rapidity gap between the leptons; charm decays produce leptons separated by nearly one unit of rapidity. However, this is not enough information to separate these pairs fully. However, as discussed in Chapter 3, the $D\overline{D}$ cross section can be obtained by measuring the correlation of opposite sign $e\mu$ pairs in the dimuon endcap and the central electron spectrometer. The acceptance of the detector system for $e\mu$ pairs as a function of rapidity, mass, transverse momentum and x_F was given in Fig. 3.7. This study was made using PISA with an event generator based on Fermilab Experiment E653 results.

The rates and acceptance for $\mu^+\mu^-$ pairs from charm decays are given in Table 3.3 and illustrated Fig. 10.6. Charm decays dominate the mass spectra below 4 GeV/c^2, but the $e\mu$ measurement should allow subtraction of the charm contribution from the dimuon spectra.

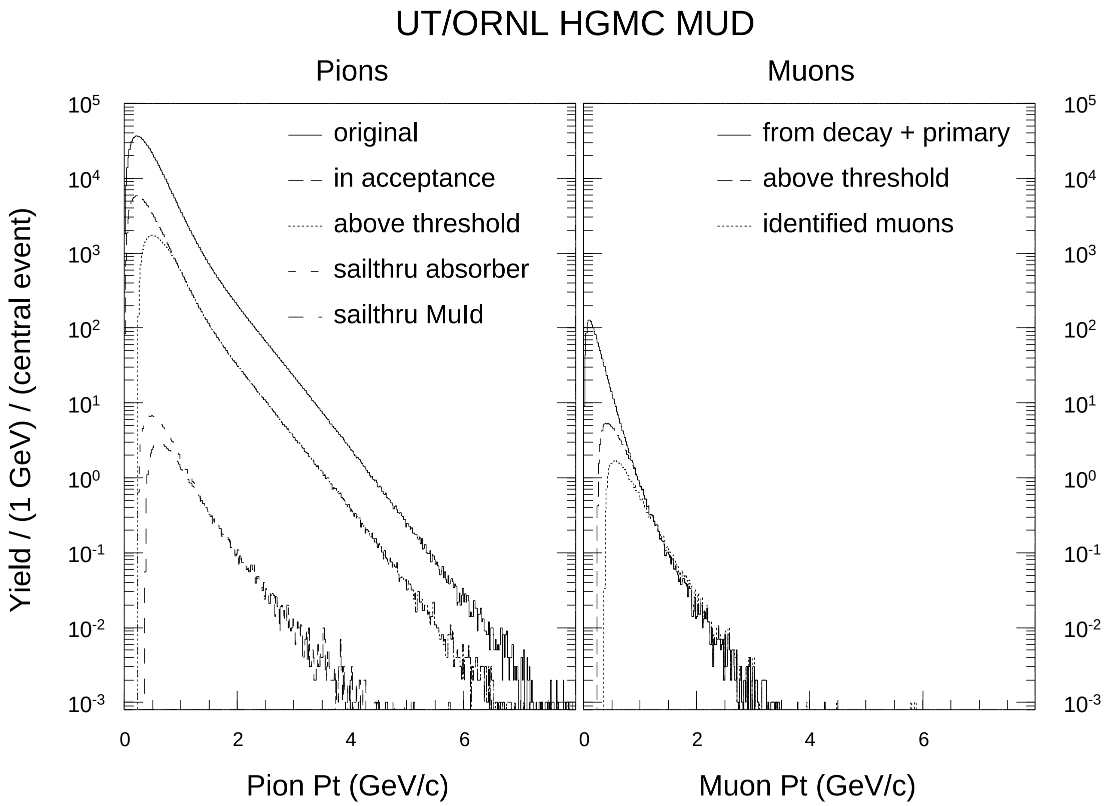

Figure 10.40: The p_T distributions of pions (left) and muons (right) at various positions in the muon detector. Absorber leakage is not included in this calculation.

An extrapolation to lower rapidity must be employed for the e^+e^- spectra.

10.5 Cost

The cost of the muon arm is broken down by WBS item and is given in Table 10.8. Formatted WBS sheets are included in the WBS summary.

10.6 Schedule

The proposed time for the muon arm is shown in Fig. 10.41. It delineates the time required for engineering, design, analysis, prototyping, procurement, fabrication, assembly, installation, and testing of the muon arm. The installation of the muon arm is intimately related to the completion of the muon magnet. The installation of the tracking chambers and their supports must be done in concert with that of the lampshade segments of the magnet. The